Journal of Systems Engineering and Electronics
Vol. 33, No. 5, October 2022, pp.1151 – 1160

# UAV safe route planning based on PSO-BAS algorithm

ZHANG Honghong [1,2], GAN Xusheng [1,2,*], LI Shuangfeng [1,2], and CHEN Zhiyuan [1]

1. Air Traffic Control and Navigation College, Air Force Engineering University, Xi'an 710051, China;
2. National Key Laboratory of Air Traffic Collision Prevention, Xi'an 710051, China

**Abstract:** In order to solve the current situation that unmanned aerial vehicles (UAVs) ignore safety indicators and cannot guarantee safe operation when operating in low-altitude airspace, a UAV route planning method that considers regional risk assessment is proposed. Firstly, the low-altitude airspace is discretized based on rasterization, and then the UAV operating characteristics and environmental characteristics are combined to quantify the risk value in the low-altitude airspace to obtain a 3D risk map. The path risk value is taken as the cost, the particle swarm optimization-beetle antennae search (PSO-BAS) algorithm is used to plan the spatial 3D route, and it effectively reduces the generated path redun dancy. Finally, cubic B-spline curve is used to smooth the plan ned discrete path. A flyable path with continuous curvature and pitch angle is generated. The simulation results show that the generated path can exchange for a path with a lower risk value at a lower path cost. At the same time, the path redundancy is low, and the curvature and pitch angle continuously change. It is a flyable path that meets the UAV performance constraints.

**Keywords:** unmanned aerial vehicle (UAV), low-attitude airspace, mission planning, risk assessment, particle swarm optimization, beetle antennae search (BAS), cubic B-spline.

**DOI:** 10.23919/JSEE.2022.000111

## 1. Introduction

With the advance of low-altitude airspace reform, it has become a current development trend for UAVs to leave isolated airspace and enter low-altitude fusion airspace to develop diversified missions. A large number of disordered low-altitude unmanned aerial vehicles (UAVs) bring harm to ground facilities and public safety [1]. Especially with the wide use of small UAVs in urban space, there will be a large number of UAVs performing aerial photography, logistics, security, search, rescue, and other tasks over cities. Meanwhile, the complex low-altitude environment formed by irregular obstacles in dense urban space brings severe challenges to the UAV safe operation [2]. At the same time, when the UAVs run at low altitude in the city, it may fall and hurt people and vehicles, increasing the UAV accidents risk [3]. Therefore, it is necessary to plan a safe and flyable route for UAVs in the complex urban low-altitude environment, to provide technical support for UAVs low-altitude air traffic management.

Route planning is one of key UAV autonomous flight technologies. There are many mature traditional methods. Common route planning methods include the heuristic algorithm, the mathematical optimization algorithm, the potential field method, the graph theory, etc.

(i) Heuristic optimization algorithm. It is an optimization algorithm that searches for approximate optimal solutions at an acceptable computational cost. It mainly includes ant colony algorithm, genetic algorithm, and A* algorithm. Luo et al. [4] used the ant colony algorithm with positive feedback and good robustness to separate the pheromones according to the advantages and disadvantages, strengthened the pheromones with good effects, and improved the route planning speed. Bao et al. [5] proposed an improved heuristic function and local search strategy of ant colony algorithm with angle factor, it is to solve the algorithm slow convergence speed problem in 3D UAV route planning. Xu et al. [6] presented a route planning approach for rotary UAVs（R-UAVs） in a known static rough terrain environment. Considering the length, height and tuning angle of a path, the route planning of R-UAVs is described as a tri-objective optimization problem. An improved multi-objective particle swarm optimization algorithm is developed.

(ii) Mathematical optimization method. According to the established UAV route planning model, the optimization problem can be transformed into the optimal control model, and the mathematical optimization method can be used to solve it. Zhang et al. [7] proposed a sequential mixed integer linear optimization method. It could simultaneously select speed regulation, direction, and height adjustment to generate a resolution path for the complex

Manuscript received January 11, 2021.
*Corresponding author.
This work was supported by the National Natural Science Foundation of China (61601497), the Natural Science Basic Research Plan in Shaanxi Province of China (2022JM-412), and the Air Force Engineering University Principal Fund (XZJ2020005).

low-altitude multi-machine conflict problem. On the premise of route pre-planning, Sarim et al. [8] adopted the mixed integer linear programming method and then carried out fine planning to improve the route smoothness.

(iii) Potential field method. The route planning method based on the potential field constructs a virtual potential field in the airspace, generates a navigation function, and converts the aircraft motion law into the result of the force between objects. Fan et al. [9] proposed a regular hexagonal guidance method based on the artificial potential field method to improve the local minimum problem. At the same time, a relative velocity method was proposed to detect and avoid moving objects in dynamic environment.

(iv) Graph theory. The route planning method based on graph theory firstly uses the rasterization method to model the environment, and then uses the search algorithm to generate the planned path. Commonly used methods are Dijkstra algorithm, Voronoi diagram, probabilistic roadmaps, etc. Angel et al. [10] proposed a route planning of multiple trajectories for a swarm of UAVs based on 3D probabilistic road maps (PRM). In addition, machine learning [11−13], model predictive control [14,15] and game theory [16,17] were also applied in route planning, and they all had certain characteristics and advantages.

Although the current route planning method has been relatively mature, the current route planning basically takes the shortest path and the minimum threat as the performance indicators to generate the UAV flyable path. After the UAV leaves the isolated airspace and enters the national airspace, each area in the 3D space has different risk values, so it is necessary to comprehensively consider obstacle avoidance requirements and safety risk management. If the airspace itself risk is ignored, the generated path will cause hidden danger to the city safety, and the low-altitude UAV air traffic management is not used. In order to ensure the low-altitude UAVs flight safety, it is necessary to consider the urban low-altitude airspace risk assessment. The path can meet the obstacle avoidance requirements and minimizes the path risk by combining the different urban areas risk maps. In view of the above problem, this paper studies the UAV route planning in the complex low-altitude environment with regional risk assessment. According to the different city modeling area, 3D airspace risk maps are established. Combined with UAV performance constraints and obstacle avoidance requirements, a path that takes into account the urban area risks is generated based on the particle swarm optimitation-beetle antennae search (PSO-BAS). Finally, cubic B-spline is used to smooth the planned path to generate continuous curvature and smooth flyable path.

## 2. Low-altitude airspace modeling

Environmental modeling is the work that needs to be completed in the first step of UAV route planning. The establishment of the model directly affects the effect of path planning. Urban environmental obstacles are numerous, diverse and unevenly distributed. To simplify the airspace running environment, speed up the planning, the city 3D space will be discretized by using the cross grid method.

As shown in Fig. 1(a), firstly, a 3D rectangular coordinate system $O$-$XYZ$ is established, and then a 3D area $ABCD$-$EFGH$ is constructed in the coordinate system, where the $ABCD$ plane is on the $XOZ$ plane, and then the UAV's low-altitude operation airspace is placed in this 3D area, $AB$ and $AE$ are respectively equal to the length and width of the airspace where the UAV operates.

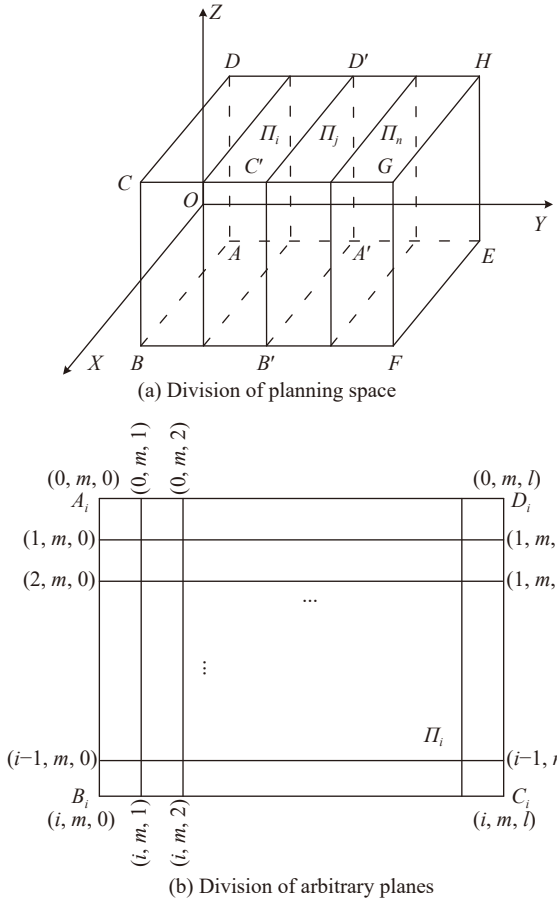


(a) Division of planning space

(b) Division of arbitrary planes

**Fig. 1 Schematic diagrams of division of planning space and arbitrary plane**

Once the planning space is obtained, it can be further divided. Firstly, $ABCD$-$EFGH$ is divided into $n$ equal parts along the $Y$ axis to obtain $(n + 1)$ planes. Then, the arbitrary plane is divided into $l$ equal parts along the $Z$ axis and $m$ equal parts along the $X$ axis, as shown in

Fig. 1(b). In this way, the planning space is discretized into $n\times m\times l$ grids. In practical applications, the division of the grid size should be based on the premise that the UAV can move freely in the unit grid, that is to say, $n$ and $m$ should be selected accordingly, and $l$ is the division in height. This can give a good balance between the environmental information amount storage and the path planning accuracy.

After the above processes, the low-altitude operation airspace of the UAV can be represented by a collection of discrete points. The airspace coordinates after rasterization correspond to the node number one by one. The coding rules can be used to convert the airspace coordinate information to the node number.

The parks, streets, buildings, residential areas, and other areas in the city low-altitude environment are regarded as static obstacles for the UAV operation. They are scattered in different areas in the city. For towering buildings, the UAV avoids collisions by flying around. For lower areas, it carries out overflight. In order to reduce the airspace structure complexity and facilitate the effective obstacle avoidance, various obstacles are simplified into cuboids.

## 3. Regional risk assessment

In the complex urban low-altitude environment, due to the differences in population density, flight height, ground cover, and other parameters of UAV operation regions, the operational risks are also greatly different. Therefore, it is necessary to conduct discrete risk assessment for each grid area and quantify risks. Each position corresponds to a risk value [18]. The $n\times m\times l$ 3D risk assessment matrix $\boldsymbol{R}$ is constructed. The risk matrix of the $k(k=1,2,\cdots,l)$ level is expressed as

$$\boldsymbol{R}_k=\begin{bmatrix} r(p_{1,1,k}) & r(p_{1,2,k}) & \cdots & r(p_{1,m,k}) \\ r(p_{2,1,k}) & r(p_{2,2,k}) & \cdots & r(p_{2,m,k}) \\ \vdots & \vdots & \ddots & \vdots \\ r(p_{n,1,k}) & r(p_{n,2,k}) & \cdots & r(p_{n,m,k}) \end{bmatrix}_{n\times m}$$

where $r(p_{i,j,k})\ (i=1,2,\cdots,n;\ j=1,2,\cdots,m;k=1,2,\cdots,l)$ represents the risk assessment value within each grid area in 3D space, and $(i,j,k)$ represents the coordinate value in 3D space.

In the 3D urban airspace, the $n\times m\times l$ UAV running path matrix can be constructed, the path matrix of the $k$th level can be expressed as

$$\boldsymbol{M}_k=\begin{bmatrix} m(p_{1,1,k}) & m(p_{1,2,k}) & \cdots & m(p_{1,m,k}) \\ m(p_{2,1,k}) & m(p_{2,2,k}) & \cdots & m(p_{2,m,k}) \\ \vdots & \vdots & \ddots & \vdots \\ m(p_{n,1,k}) & m(p_{n,2,k}) & \cdots & m(p_{n,m,k}) \end{bmatrix}_{n\times m}$$

where $m(p_{i,j,k})\ (i=1,2,\cdots,n;\ j=1,2,\cdots,m;k=1,2,\cdots,l)$ represents whether each grid area in the 3D space is flown over by the UAV, denoted as

$$m(p_{i,j,k})=\begin{cases} 1, & \text{UAV fly over the grid} \\ 0, & \text{UAV bypass the grid} \end{cases}.$$

Therefore, the cost of considering regional risk assessment is expressed as

$$C=\sum_{i,j,k} r(p_{i,j,k})m(p_{i,j,k}). \tag{1}$$

The lower the risk assessment value, the less security threat the path poses. At present, the mortality rate is usually used as a method to evaluate the risk UAV operation [19–21]. The risk assessment value calculation process in each grid area is described below.

### 3.1 Risk assessment of UAV impact on humans

Due to the high people density in urban space and the high value of ground property, the UAV falling accident often causes higher loss of people and property. Therefore, urban route planning considering regional risk assessment can plan a path with lower risk value for UAVs. It can reduce operational risk to a certain extent. UAVs operating in urban space pose a certain threat to ground personnel due to their reliability and the difference in operating areas. Currently, UAVs are mainly represented by accident fatality rate [22] of UAV system:

$$P_1=f_G N_{\exp} P(f) \tag{2}$$

where $f_G$ represents the UAV reliability index, it represents the system crash rate due to its own failure; $N_{\exp}$ represents the people number exposed to the UAV ground impact accident; $P(f)$ represents the death rate of the system impact. $N_{\exp}$ can be expressed as

$$N_{\exp}=A_{\exp}\rho \tag{3}$$

where $\rho$ represents population density; $A_{\exp}$ represents the killing area of ground collision when the UAV system falls down. Combined with [23], $A_{\exp}$ is related to the UAV itself physical properties and the sliding parameters, as shown in Fig. 2. It is expressed as

$$A_{\exp}=2(r_p+R_{\text{uav}})d+\pi(r_p+R_{\text{uav}})^2 \tag{4}$$

where $r_p$ represents the ground personnel radius; $R_{\text{uav}}$ represents the UAV maximum radius. According to the geometric relationship in Fig. 2, $d=h_p/\tan\theta$, where $\theta$ represents the UAV sliding and falling angle, and it can be determined by the following formula:

$$\begin{cases} \theta=\arctan\left(\dfrac{V_y}{V_{\max}}\right) \\ a=\dfrac{mg-F_d}{m}=g-\dfrac{R_I A\rho_A v_{\text{rel}}^2}{2m} \\ V_y=\displaystyle\int_0^t a\mathrm{d}t=\sqrt{\dfrac{2mg}{R_I A\rho_A}\left(1-\mathrm{e}^{-\frac{hR_I A\rho_A}{2m}}\right)} \end{cases} \tag{5}$$

where $V_y$ and $V_{\max}$ respectively indicate the UAV fall vertical speed and their own maximum speed; $F_d$ represents the UAV air resistance during it falls, $g$ represents gravitational acceleration, $R_I$ represents the drag correlation coefficient, it is associated with its physical properties; $A$ represents the UAV area; $\rho_A$ represents air density; $v_{\text{rel}}$ represents the UAV actual airspeed when it crashes.

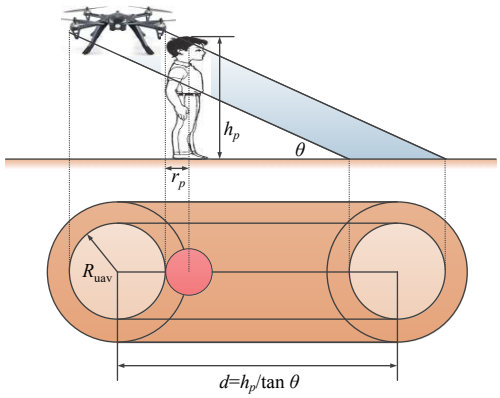


**Fig. 2 Schematic diagram of the killing area of falling UAV**

The UAV impact fatality rate $P(f)$ can be expressed as

$$P(f)=\frac{1}{1+\sqrt{\frac{\alpha}{\beta}}\left(\frac{\beta}{E_{\text{imp}}}\right)^{\frac{1}{4p_s}}} \tag{6}$$

where $E_{\text{imp}}$ represents the impact kinetic energy and it is calculated with $E_{\text{imp}}=(1/2)mV_{\text{imp}}^2$, $V_{\text{imp}}=\sqrt{V_{\max}^2+V_y^2}$; $\alpha$ is defined as the required impact capacity when the mortality rate reaches 50% when $p_s$ is set as 0.5; $\beta$ is defined as the impact capacity critical value for the death events when $p_s$ is set as 0. Shading parameter $p_s$ represents the impact degree of UAV system ground impact event on urban ground personnel, and its value is between [0,1]. The larger the value is, the better the ground shelter effect is. According to the actual situation of urban ground shelter effect, the various types shelter parameter settings of areas are shown in Table 1.

**Table 1 Masking parameters**

| Coefficient | Shelter parameter |
|---|---|
| 0 | No shelter |
| 0.25 | Sparse trees |
| 0.50 | Trees or low buildings |
| 0.75 | High-rise building |
| 1 | Industrial zone |

### 3.2 Risk assessment of UAV impact on vehicle

During the UAVs operation in cities, due to the numerous towering buildings, the planned flying path is often over the road. The UAVs fall down due to a failure and collide with vehicles on the ground, causing traffic accidents and injuries. Therefore, in the urban 3D route planning process, it is necessary to consider the risk assessment of UAV impact on vehicles.

The expected death rate of a UAV hitting a ground vehicle can be defined as the deaths number per hour caused by the UAV falling, it can be expressed as

$$P_2=f_G CT \tag{7}$$

where $T$ represents the average deaths number caused by each traffic accident; $C$ represents the UAV hitting the vehicle probability. $C$ can be defined by the ratio of the all vehicles projected total area to the covered road total area:

$$C=\frac{\bar{S}_{\text{car}}N}{S_{\text{road}}} \tag{8}$$

where $\bar{S}_{\text{car}}$ represents the vehicles projected area on the ground, $N$ represents the vehicles number calculated by $N=KL$, $K$ represents the traffic density (the vehicles number on the road per unit length), $L$ represents the road length, $S_{\text{road}}$ represents the road area calculated by $S_{\text{road}}=D_{\text{road}}L$, and $D_{\text{road}}$ represents the road width.

### 3.3 Three-dimensional route planning model considering regional risk assessment

If regional risks are not taken into account, the property index of urban airspace air route planning is $J_0=\omega_1 J_l+\omega_2 J_s$. If regional risks are taken into account, the performance indicators of urban airspace route planning is expressed as $J_0'=C=\sum_{i,j,k} r(p_{i,j,k})m(p_{i,j,k})$.

Small UAVs flying in urban space are limited by their own performance, and they often cause safety hazards when performing large maneuvers. Therefore, flight constraints and terrain constraints need to be considered in the planning process.

(i) The maximum horizontal turning angle. Limited by its own hardware performance, when the UAV turns in a horizontal direction, the turning angle cannot exceed the maximum horizontal turning angle $\Delta\psi_{\max}$. Assume that in $N$ path assembly points, and the $n$th horizontal turning angle track segment compared to the $(n-1)$th track segment is $\Delta\psi_n$. Then, the horizontal turning angle constraint is

$$|\Delta\psi_n|\leqslant\Delta\psi_{\max},\quad n=1,2,\cdots,N. \tag{9}$$

(ii) The maximum pitch angle. Pitch angle refers to the angle when the UAV climbs up or dives down. Due to performance limitations, the high and low angle of the UAV in flight cannot exceed the maximum high and low angle $\theta_{\max}$. Assuming that in $N$ path assembly points, the

pitch angle between the $n$th track segment and the $(n-1)$th track segment is $\theta_k$, then the maximum pitch angle constraint is

$$|\theta_n| \leqslant \theta_{\max},\ \ n = 1,2,\cdots,N. \tag{10}$$

(iii) Terrain constraints. The flight altitude and terrain altitude should meet the safety threshold requirements, and the terrain constraints can be expressed as

$$H_{\text{safe}} - \min(z_n - H_{\text{ter}}) \leqslant 0 \tag{11}$$

where $H_{\text{safe}}$ is the safety threshold; $H_{\text{ter}}$ is the terrain height where the waypoint is located; $z_n$ is the flight height of the $n$th track segment in the flight path.

The total flight path risk value in the urban airspace is used as the objective function, and obstacles such as non-flyable buildings in the low-altitude airspace are used as path constraints. The parameter that needs to be optimized in the UAV route is the set point of the planned path. Therefore, the 3D path model can be simplified to the following expression, and the model considers the urban low-altitude areas risk assessment:

$$\min J_0' = \min C = \min \sum_{i,j,k} r(p_{i,j,k}) m(p_{i,j,k})$$

$$\text{s.t.} \begin{cases} r(p_{i,j,k}) = P_1 + P_2 \\ m(p_{i,j,k}) = \begin{cases} 1, & \text{UAV flies over the grid} \\ 0, & \text{UAV bypasses the grid} \end{cases} \\ |\Delta\psi_n| \leqslant \Delta\psi_{\max},\ \ n = 1,2,\cdots,N \\ |\theta_n| \leqslant \theta_{\max},\ \ n = 1,2,\cdots,N \\ H_{\text{safe}} - \min(z_n - H_{\text{ter}}) \leqslant 0 \end{cases}. \tag{12}$$

## 4. 3D route planning based on PSO-BAS algorithm

### 4.1 Standard PSO

PSO is an optimization algorithm. It simulates the birds random predatory phenomena. Each particle can be regarded as a bird, it will have individual and group information feedback in the predation process. Each bird represents a possible solution to the optimization problem. When a bird finds food, other birds in the group will move towards it. PSO algorithm is to use the birds' information sharing characteristics to form a process from dispersion to concentration. All particles have a fitness value determined by the optimized function, and each particle has a speed to determine the direction and its flight distance. The algorithm initializes a group of random particles (random solutions), and then searches for the optimal solution through iterative updating. In the PSO algorithm, each particle has a memory to track the previous generation optimal position during iteration: one is the optimal position found by the particle itself. It is called the particle individual optimal position. The other is the optimal position found by the whole group. It is called the particle global optimal position.

It is assumed that there are $N$ particle in the $D$-dimensional search space, that is, the particle swarm population size is $N$, the $i$ th particle position parameter in the $D$-dimensional can be expressed as $x_i(k) = (x_{i1}(k), x_{i2}(k), \cdots, x_{iD}(k))$. The optimization problem cost function is used to determine whether the particle current position is better than the historical position.

Up to now, the $i$ th particle individual optimal value position parameter $p_{\text{best}}$ is

$$p_{\text{best}} = (p_{i1}, p_{i2}, \cdots, p_{iD}). \tag{13}$$

Up to now, the optimal population value position parameter $g_{\text{best}}$ for all particles is

$$g_{\text{best}} = (p_{g1}, p_{g2}, \cdots, p_{gD}). \tag{14}$$

The velocity is

$$v_i(k) = (v_{i1}(k), v_{i2}(k), \cdots, v_{iD}(k)). \tag{15}$$

The $i$ th particle velocity and position iteration rule at the $k$ time is

$$\begin{cases} v_i(k+1) = \omega v_i(k) + c_1 r_1 (p_{\text{best},i}(k) - x_i(k)) + \\ \qquad c_2 r_2 (g_{\text{best}}(k) - x_i(k)) \\ x_i(k+1) = x_i(k) + v_i(k+1) \end{cases}. \tag{16}$$

where $k$ is the iterations number, $\omega$ is the inertia weight; $c_1$ and $c_2$ are the acceleration factors. It mainly controls the individual information feedback and group information communication of particles. It enables particles to make judgments based on the information obtained by the individual and group optimization, adjust their own positions and approach the potential optimal position. $r_1$ and $r_2$ are random numbers from 0 to 1. They increase the fault tolerance and particles optimization ability.

### 4.2 BAS algorithm

The BAS algorithm was put forward in 2017 based on the beetle antennae foraging principle. It mainly detects food smell based on the beetle antennae tentacles and determines its own direction. If a higher odor concentration is detected on one side of the antenna, the beetle will rotate in the same direction. Otherwise it will turn to the other side. BAS algorithm flow is as follows:

**Step 1** For the $m$-dimensional optimization problem, the centroid is expressed as $\boldsymbol{x}$, left-whisker $\boldsymbol{x}_l$, right-whisker $\boldsymbol{x}_r$, and two-whisker distance $d$. $\boldsymbol{x}$, $\boldsymbol{x}_l$, and $\boldsymbol{x}_r$ are all $m$-dimensional vectors.

**Step 2** Because the beetle head orientation is random, a random $m$-dimensional unit vector is generated to represent the vector that the left whisker points to the right whisker

$$\boldsymbol{b}=\frac{\text{rands}(m,1)}{\|\text{rands}(m,1)\|} \tag{17}$$

where rands(·) stands for random function.

The relation between the left and right whiskers and the mass center spatial coordinates is

$$\begin{cases}\boldsymbol{x}_l=\boldsymbol{x}^t+d^t\cdot\boldsymbol{b}\\ \boldsymbol{x}_r=\boldsymbol{x}^t-d^t\cdot\boldsymbol{b}\end{cases} \tag{18}$$

where $d^t$ represents the distance between the two whiskers in the $t$th iteration. $\boldsymbol{x}^t$ represents the beetle centroid position in the $t$th iteration.

**Step 3** Calculate the fitness values $f(\boldsymbol{x}_l)$ and $f(\boldsymbol{x}_r)$ of the left and right whiskers $\boldsymbol{x}_l$ and $\boldsymbol{x}_r$, and judge the beetle direction according to the size relationship between $f(\boldsymbol{x}_l)$ and $f(\boldsymbol{x}_r)$.

$$\boldsymbol{x}^t=\boldsymbol{x}^{t-1}-\delta^t\boldsymbol{b}\text{sign}(f(\boldsymbol{x}_l)-f(\boldsymbol{x}_r)) \tag{19}$$

where sign (·) is the symbolic function, and $\delta^t$ is the step size of the $t$th iteration.

**Step 4** Calculate the fitness value after the beetle movement, and update the distance and step size between the left and right whisker

$$d^t=\text{eta\_}d\cdot d^{t-1}, \tag{20}$$

$$\delta^t=\text{eta\_}\delta\cdot\delta^{t-1}, \tag{21}$$

where $d^t$ is the distance between the two whiskers in the $t$th iteration; eta_$d$ and eta_$\delta$ are the two-whisker distance and the step size decay coefficient respectively.

**Step 5** Judge whether the iteration end condition is met. If yes, end the iteration; otherwise repeat Steps 2−4 until the condition is met.

### 4.3 PSO-BAS algorithm

The BAS algorithm biggest limitation is its individual singleness. When a certain iterations number is reached, the step size attenuation will lead to the beetles movements in all directions that are too small. Therefore, it is difficult to jump out after falling into the local optima. Using a fixed step or a larger initialization step may skip the best and easily lead to unstable results. With the information sharing characteristic among the PSO particles, a PSO-BAS algorithm is proposed in this paper. In this algorithm, the PSO individual optimal value comparison process is changed to BAS optimization, so as to update the individual and global optimal value [24,25].

The PSO algorithm function is to make the "beetle" distribution more dispersed. It is to make all close to the optimal value through the different particles information exchange. At the same time, changing the PSO comparison process to BAS for further optimization can better improve the convergence speed and prevent premature local optimization due to convergence. The algorithm specific process is described as follows:

**Step 1** Initialize the population size, speed and position of particles.

**Step 2** Evaluate the fitness of each particle.

**Step 3** Update individual and global optimality through BAS.

**Step 4** The PSO approaches dominant particle in (16) to the global optima.

**Step 5** Update the BAS parameters.

**Step 6** Judge whether the accuracy standard is met. If the iterations maximum number is not met, then turn to Step 2.

### 4.4 Cubic B-spline smoothing path

The urban space 3D route planning obtained based on PSO-BAS algorithm basically satisfies the UAV constraint conditions. However, in the actual flight process, the planned flight path often has sharp angles and discontinuous curvature, so it is necessary to conduct smoothing processing on the flight path to generate a smooth and flyable 3D path. B-spline is a special case of Bezier curve. By approximating the polygon, a smooth curve can be obtained. Since it has continuity and will not affect the global situation when changing control points position, it has been widely used in track smoothing [26].

Given $(n+1)$ control points $P_i(i=0,1,\cdots,n)$, then $n$ times uniform B-spline curve can be expressed as

$$Qn(t)=\sum_{i=0}^{n}B_{i,n}(t)P_i \tag{22}$$

where $B_{i,n}(t)$ is the $n$-order ($n$-1) degree B-spline curve basis function. The B-spline curve is composed of curve segments, and adjacent curves have the same control points. The definition of $B_{i,n}(t)$ [26] can be expressed as

$$B_{i,0}(t)=\begin{cases}1, & t_i\leqslant t\leqslant t_{i+1}\\ 0, & \text{else}\end{cases}, \tag{23}$$

$$B_{i,n}(t)=\frac{t-t_i}{t_{i+n}-t_i}B_{i,n-1}(t)+\frac{t_{i+n+1}-t}{t_{i+n+1}-t_{i+1}}B_{i+1,n-1}(t),\ \ n\geqslant 1. \tag{24}$$

In order to facilitate local curve control, cubic B-spline curve is selected to smooth the UAV track. The matrix can be expressed as

$$S_i(t)=\frac{1}{6}\begin{bmatrix}t^3 & t^2 & t & 1\end{bmatrix}\cdot\begin{bmatrix}-1 & 3 & -3 & 1\\ 3 & -6 & 3 & 0\\ -3 & 0 & 3 & 0\\ 1 & 4 & 1 & 0\end{bmatrix}\begin{bmatrix}P_0\\ P_1\\ P_2\\ P_3\end{bmatrix}. \tag{25}$$

Cubic B-spline curve formula is used to generate a smooth track curve with continuous curvature. It satisfies UAV performance constraints, as shown in Fig. 3. The

blue line is the track obtained after cubic B-spline curve smoothing processing.

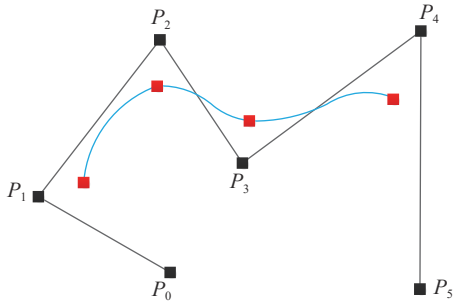


**Fig. 3 Cubic B-spline curve smoothing processing**

## 5. Simulation analysis

In order to verify the effectiveness and applicability of the urban low-altitude UAV flight route planning considering regional risk assessment proposed in this paper. The Xidian University North Campus is selected as the UAV track planning background. The satellite image is shown in Fig. 4, and the starting and ending positions are marked.


**Fig. 4 Map of Xidian University North Campus**

The route planning method flow chart considering regional risk assessment is shown in Fig. 5.

Since the same area has great differences in parameters in different time periods, the parameters are selected to refer to a specific moment instantaneous value in the route planning scene during the simulation process. It can be estimated by historical data. The parameters required for risk assessment in this planning scenario are shown in Table 2. The parameters required for the PSO-BAS algorithm are shown in Table 3.

According to the planning method proposed in this paper, the risk value in the low-altitude airspace is evaluated, and then the comprehensive cost value required by the UAV route planning is comprehensively considered to generate discrete path points. Finally, cubic B-spline curve is used to smooth the path to obtain the UAV flyable path, as shown in Fig. 6.

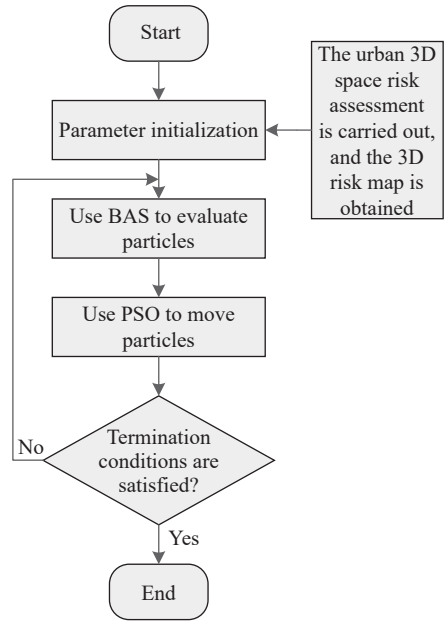


**Fig. 5 Route planning process based on PSO-BAS**

**Table 2 Values of regional risk assessment parameters**

| Parameter | Value | Parameter | Value |
|---|---|---|---|
| $f_G/\mathrm{h}^{-1}$ | $6.4\times10^{-5}$ | $\rho_A/(\mathrm{kg/m}^3)$ | 1.225 |
| m/kg | 1.38 | $\beta$/J | 34 |
| $\rho/\mathrm{km}^{-2}$ | 30 000 | $R_I$ | 0.3 |
| $r_p$/m | 0.25 | $\bar{S}_{\mathrm{car}}/\mathrm{m}^2$ | 8.4 |
| $h_p$/m | 1.65 | $K$ | 0.1 |
| $R_{\mathrm{uav}}$/m | 0.2 | $D_{\mathrm{road}}$/m | 3 |
| $v_{\max}/(\mathrm{m/s})$ | 16 | $T$ | 3 |
| $g/(\mathrm{m/s}^2)$ | 9.8 | $H_{\mathrm{safe}}$/m | 3 |
| $A/\mathrm{m}^2$ | 0.018 8 | — | — |

**Table 3 PSO-BAS algorithm required parameters**

| Parameter | Value | Parameter | Value |
|---|---|---|---|
| $N$ | 20 | $c_1$ | 1.5 |
| $\omega_1$ | 0.5 | $c_2$ | 2 |
| $\omega_2$ | 0.2 | $m$ | 3 |
| $k$ | 200 | eta_$d$ | 0.95 |
| $\omega$ | 1 | eta_$\delta$ | 0.95 |

In order to verify whether the spatial curve satisfies the UAV maneuvering performance constraints, the smoothing spatial track is divided into horizontal and vertical directions. The UAV maximum pitch angle and turning radius are determined by calculating the curve derivative respectively. As shown in Fig. 7 and Fig. 8, the step size is one coding counting unit, the spatial track curvature is continuous, and the curvature value is less than 1, and the spatial track pitch angle is less than $\pi/4$. It conforms to

the UAV performance constraints. Therefore, the path obtained after smoothing processing can be used for the UAV actual flight.

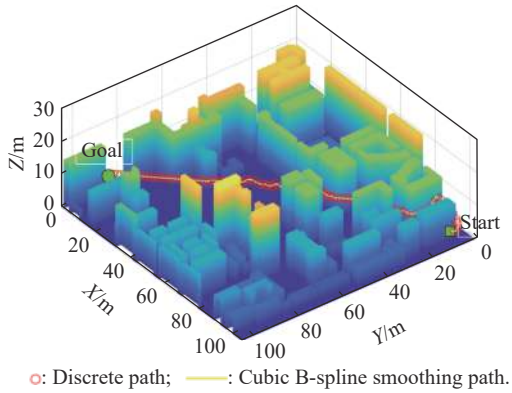


**Fig. 6 Schematic diagram of low-altitude airspace route planning**

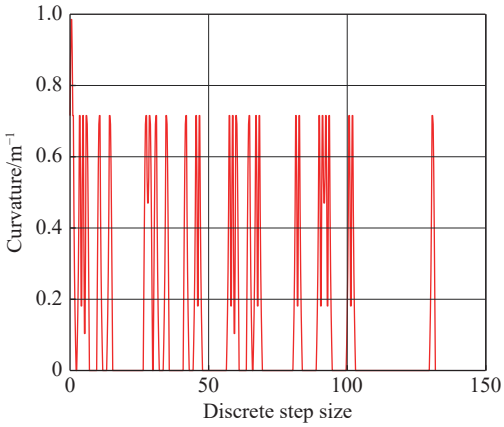


**Fig. 7 Curvature change of space track**

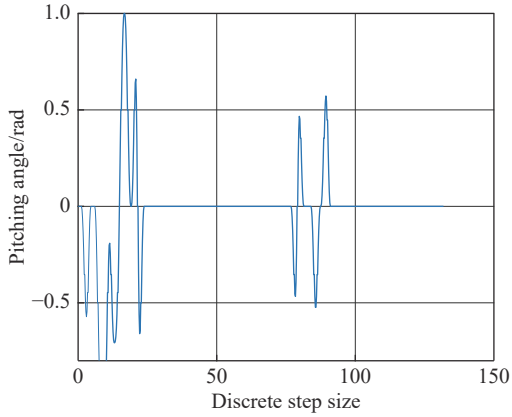


**Fig. 8 Spatial track elevation angle variation**

In order to verify the PSO-BAS algorithm superiority proposed in this paper, the PSO-BAS algorithm is compared with the paths planned by the PSO algorithm, ant colony optimization (ACO) algorithm, and PSO-ACO. The results are shown in Fig. 9. The path risk value trend with the iterations number is shown in Fig. 10. After improvement, the PSO-BAS algorithm completes the search process at 55 iterative times. It is faster than other algorithms. At the same time, the cost risk value tends to stabilize, reaching $8.75\times10^{-7}$, and the optimization is also stronger than other algorithms. Therefore, it can be concluded that the PSO-BAS algorithm can quickly plan the flyable path, and at the same time can effectively reduce the redundancy, reduce the risk value, and improve the planning effect.

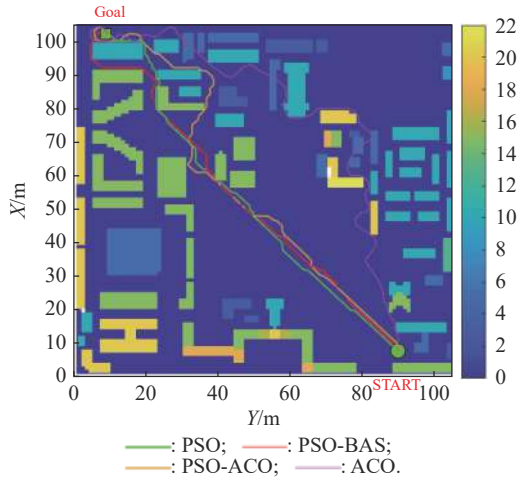


**Fig. 9 Comparison of different planning algorithm tracks**

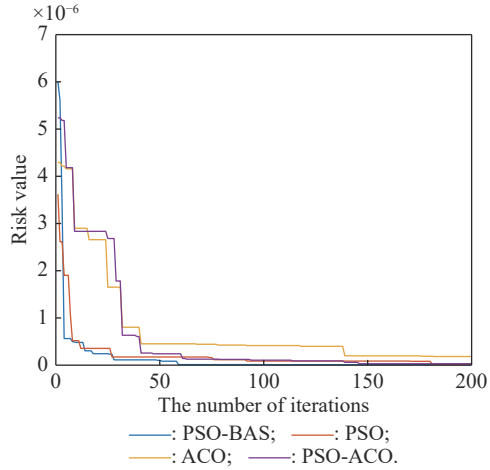


**Fig. 10 Search process of different solving algorithms**

The path risk value and path length in the planning method considering risk assessment and the planning method without risk assessment are compared. The results are shown in Table 4, and the analysis show that the planning method considering risk assessment through additional pay 15% of the path cost, in return for 86% lower risk value of the safe path, and it is helpful for UAV in complex low safe operation environment.

**Table 4 Performance comparison of route planning methods**

| Type | Path risk value | Path length/m |
|---|---|---|
| Planning methods considering risk assessment | $8.75\times10^{-7}$ | 156.74 |
| Planning methods without considering risk assessment | $6.45\times10^{-6}$ | 136.48 |

## 6. Conclusions

In this paper, a relatively safe and smooth UAV flying path is planned based on the characteristics of complex urban low-altitude airspace and regional risk assessment. Aiming at many kinds of obstacles characteristics and high uncertainty in urban low-altitude airspace, a complex low-altitude environment containing dense obstacles is constructed to operate close to the actual city. In view of the threat posed by UAV crash to urban space with high density of people and property, based on regional risk assessment, the path risk value is considered in the route planning process to generate a relatively safe planning path. Aiming at the problem that the discrete path precision generated by PSO algorithm is not enough, the PSO-BAS algorithm is proposed, and the path is smoothed by cubic B-spline curve to get flyable paths that meet the UAV performance constraints.

## References


[1] QUAN Q, LI G, BAI Y Q, et al. An overview and suggestions on traffic management of low-altitude UAV. Acta Aeronautica et Astronautica Sinica, 2020, 41(1): 6–34. (in Chinese)

[2] ZHANG Q R, WEI R X, HE R K, et al. Flight path planning of urban dense irregular obstacle space UAV. Control Theory & Applications, 2015, 32(10): 1407–1413. (in Chinese)

[3] LEVASSEUR B, BERTRAND S, RABALLAND N, et al. Accurate ground impact footprints and probabilistic maps for risk analysis of UAV missions. Proc. of the IEEE Aerospace Conference, 2019. DOI: 10.1109/AERO.2019.8741718.

[4] LUO Q, WANG H B, ZHENG Y, et al. Research on path planning of mobile robot based on improved ant colony algorithm. Neural Computing and Applications, 2020, 32(6): 1555–1566.

[5] BAO S T, LU Y G, et al. Research on path planning of UAV based on ant colony algorithm with angle factor. Journal of Physics: Conference Series, 2020, 1627(1): 1–8.

[6] XU Z, ZHANG E Z, CHEN Q W. Rotary unmanned aerial vehicles path planning in rough terrain based on multi-objective particle swarm optimization. Journal of Systems Engineering and Electronics, 2020, 31(1): 130–141.

[7] ZHANG Q Q, WANG Z Y, ZHANG H H, et al. A complex low-altitude multi-aircraft conflict resolution method based on SMILO-VTAC model. Journal of Traffic and Transportation Engineering, 2019, 19(6): 125–136. (in Chinese)

[8] SARIM M, RADMANESH M, DECHERING M, et al. Distributed detect-and-avoid for multiple unmanned aerial vehicles in national airspace. Journal of Dynamic Systems, Measurement and Control, 2019, 141(7): 071014.

[9] FAN X J, GUO Y J, LIU H, et al. Improved Artificial Potential Field Method Applied for AUV Path Planning. Mathematical Problems in Engineering, 2020: 6523158. DOI: 10.1155/2020/6523158.

[10] ANGEL M, ABDULLA A, DAVID M, et al. 3D Trajectory planning method for UAVs swarm in building emergencies. Sensors, 2020, 20(3): 642.

[11] ZHANG Y Y, LI S, GUO H L. A type of biased consensus-based distributed neural network for path planning. Nonlinear Dynamics, 2017, 89: 1803–1815.

[12] CHANG Y, WANG Y Q, ALSAADI F E, et al. Adaptive fuzzy output-feedback tracking control for switched stochastic pure-feedback nonlinear systems. International Journal of Adaptive Control and Signal Processing, 2019, 33(10): 1567–1582.

[13] GAO X, FANG Y W, WU Y L. Fuzzy Q learning algorithm for dual-aircraft path planning to cooperatively detect targets by passive radars. Journal of Systems Engineering and Electronics, 2013, 24(5): 800–810.

[14] ALEXANDRA G, ESTEN I G, DAC-TU H, et al. UAVs trajectory planning by distributed MPC under radio communication path loss constraints. Journal of Intelligent and Robotic Systems, 2015, 79(1): 115–134.

[15] WU J F, WANG H L, LI N, et al. Distributed trajectory optimization for multiple solar-powered UAVs target tracking in urban environment by adaptive grasshopper optimization algorithm. Aerospace Science and Technology, 2017, 70: 497–510.

[16] GUAN X M, LU R L. A conflict resolution method for complex low-altitude flight based on satisfactory game theory. Acta Aeronautica et Astronautica Sinica, 2017, 38(S1): 120–128. (in Chinese)

[17] SISLAK D. Agent-based cooperative decentralized airplane-collision avoidance. IEEE Trans. on Intelligent Transportations Systems, 2011, 12(1): 36–46.

[18] PRIMATESTA S, GUGLIERI G, RIZZO A. A risk aware path planning strategy for UAVs in urban environments. Journal of Intelligent & Robotic Systems, 2019, 95(2): 629–643.

[19] ZHANG H H, GAN X S, WU Y R, et al. Evaluation of safety target level of UAV system based on Monte-Carlo. http://kns.cnki.net/kcms/detail/41.1227.TN.20201016.0848.002.html. (in Chinese)

[20] HU X T, WU YU. Risk-based discrete multi-path planning method for UAVs in urban environments. http://kns.cnki.net/kcms/detail/11.1929.V.20200821.1328.006.html.

[21] KOH C H, LOW K H, LI L, et al. Weight threshold estimation of falling UAVs (unmanned aerial vehicles) based on impact energy. Transportation Research Part C: Emerging Technologies, 2018, 93: 228–255.

[22] ZHANG Z J, ZHANG S G, LIU X, et al. Estimated method of target level of safety for unmanned aircraft system. Journal of Aerospace Power, 2018, 33(4): 1017–1024. (in Chinese)

[23] ZHANG X J, LIU Y, ZHANG Y. Safety Assessment and Risk Estimation for Unmanned Aerial Vehicles Operating in National Airspace System. Journal of Advanced Transportation, 2018: 4731585. DOI: 10.1155/2018/4731585.

[24] LI Q H, WEI A X, ZHANG Z H. Application of economic load distribution of power system based on BAS-PSO. IOP Conference Series: Materials Science and Engineering, 2019, 490(7): 2727.

[25] FAN Y Q, SHAO J P, SUN G T. Optimized PID controller based on beetle antennae search algorithm for electro-hydraulic position servo control system. Sensors, 2020, 902: 54–64.

[26] NGOC H T, ANH D N, THANH N N. A genetic algorithm application in planning path using B-Spline model for autonomous underwater vehicle (AUV). Applied Mechanics and Materials, 2020, 4796: 54–64.

## Biographies

**ZHANG Honghong** was born in 1995. He received his B.S. degree in 2018 from Air Force Engineering University, now he is a master's student of Air Force Engineering University. His main research interests include UAV mission planning and safety assessment.
E-mail: anhuifuyangzhh@sina.com

**GAN Xusheng** was born in 1971. He received his B.S. degree in 1997 from Air Force Engineering College, M.S. degree in 2004 from Air Force Engineering University, and Ph.D. degree in 2008 from Northwestern Polytechnical University. Now he is an associate professor of the Air Force Engineering University. His main research interests include UAV air traffic management and air traffic control.
E-mail: gxsh15934896556@qq.com

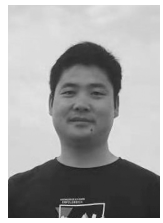

**LI Shuangfeng** was born in 1980. He received his doctorate in combat command from the Air Force Command Academy in 2014. His research direction is combat command and air traffic control.
E-mail: 77625747@qq.com

**CHEN Zhiyuan** was born in 1993. He received his B.S. degree in 2016 from Air Force Engineering University, now he is a master's student of Air Force Engineering University. His main research interests include air traffic management and safety.
E-mail: 838115488@qq.com